Nano Research Energy

ISSN 2791-0091 (print); 2790-8119 (online)
https://doi.org/10.26599/NRE.2025.9120159

Research Article

Multi-carbonyl naphthalene diimide polymer as a high-performance cathode for stable lithium-ion storage

Hewei Luo[1] (✉), Feigen Xiong[1], Haonan Bai[1], Chen Wang[1], Yang Wang[1], Kang Zhao[1], Ji Yan[1], Yong Zhang[1], Junwei Ding[1], Shiwen Wang[1], Linsen Zhang[1], Juchen Guo[2] (✉), and Zitong Liu[3] (✉)

[1] *Collaborative Innovation Center for New Energy Vehicle of Henan Province, Henan International Joint Laboratory of Ceramic Energy Materials, College of New Energy, Zhengzhou University of Light Industry, Zhengzhou 450002, China*
[2] *Department of Chemical and Environmental Engineering and Materials Science and Engineering Program, University of California, Riverside, CA 92521, USA*
[3] *State Key Laboratory of Applied Organic Chemistry, College of Chemistry and Chemical Engineering, Lanzhou University, Lanzhou 730000, China*

Received: 23 January 2025 / **Revised:** 26 February 2025 / **Accepted:** 28 February 2025 / **Published date:** 19 March 2025

ABSTRACT

Organic materials are emerging candidates for lithium-ion batteries. Unfortunately, limited electrical conductivity and high solubility in organic electrolytes usually cause low capacity and short cycle life, which hinder the utilization of organic materials. Herein, a novel multi-carbonyl naphthalene diimide non-conjugated polymer (NDI-BU) has been readily synthesized through one-step reaction. The designed polymer structure of NDI-BU shows a long and flat discharge platform. The abundant carbonyls provide multiple reaction sites for lithium ions, and resulting in a high specific capacity of 308 mAh·g^{-1} at 0.2C. An incredibly long cycle life of 20,000 cycles at 5C with 82% capacity retention is achieved. This work may inspire the effective design strategy for high energy density organic cathode materials.

KEYWORDS

lithium-ion battery, multi-carbonyl, naphthalene diimide, organic electrode, polymer

1 Introduction

Lithium-ion batteries (LIBs) have been extensively used for energy storage and power devices because of their excellent cycle stability and high energy density [1–4]. However, LIBs with transition-metal oxide cathodes are reaching their capacity limits and facing the challenge of transition-metals shortage [5]. Organic compounds containing only C, H, N, O, and other light elements are promising candidates for high capacity, sustainable, and environmentally friendly LIBs [6–8]. The capacity, conductivity, and discharge voltage of organic electrodes can be tuned by changing molecular structure to achieve high performance LIBs [9, 10]. Furthermore, LIBs with organic electrodes could be used for wearable devices due to their flexibility [11, 12].

To date, many organic electrodes with excellent performance have been developed such as 2D polyarylimide (2D-PAI) [13], cyclohexanehexone (C_6O_6) [14], quinoxaline-based heteroaromatic molecules (3Q) [15], dihydroxyanthraquinone (LiDHAQS) [16] and copper-benzoquinoid metalorganic framework (Cu-THQ MOF) [17]. Among the techniques to synthesize organic electrodes, polymerization is an effective method for preventing dissolution of active materials in organic electrolytes [18]. But this technique has several drawbacks as well. First, a sloping cell voltage profile usually appears when using conjugated polymer cathodes because the redox units strongly affect each other electronically [19]. Second, polymerization causes low capacity and conductivity if the repeat units are linked by non-electroactive groups [20]. Therefore, how to improve the specific capacity and ensure a flat discharge plateau is particularly important for organic polymer cathodes.

Organic carbonyl compounds, such as perylene tetracarboxylic diimide (PDI) [21, 22], quinone [23, 24], naphthalene tetracarboxylic diimide (NDI) [25, 26], and benzoyl compounds [27, 28] have emerged as high-performance organic electrode materials because of their high capacity and electrochemical stability. Among them, NDI shows flat discharge plateau, stable redox molecular structure and long cyclability [29, 30]. However, the capacity of NDI compounds is often lower than 250 mAh·g^{-1} due to their low electroactive sites per molecule [31]. On the other hand, small molecules with multiple carbonyl moieties may have high specific capacity, but high solubility in organic electrolytes. Thus, we propose combining carbonyl and NDI repeat units to synthesize non-conjugated polymers as new LIB cathodes with both high specific capacity and stable cycling performance.

Based on this hypothesis, we synthesized a novel non-conjugated polymer (NDI-BU, Fig. 1(a)), in which four carbonyl moieties per repeat unit are electrochemically active towards

Address correspondence to Hewei Luo, luohw@zzuli.edu.cn; Juchen Guo, juguo@ucr.edu; Zitong Liu, liuzt@lzu.edu.cn

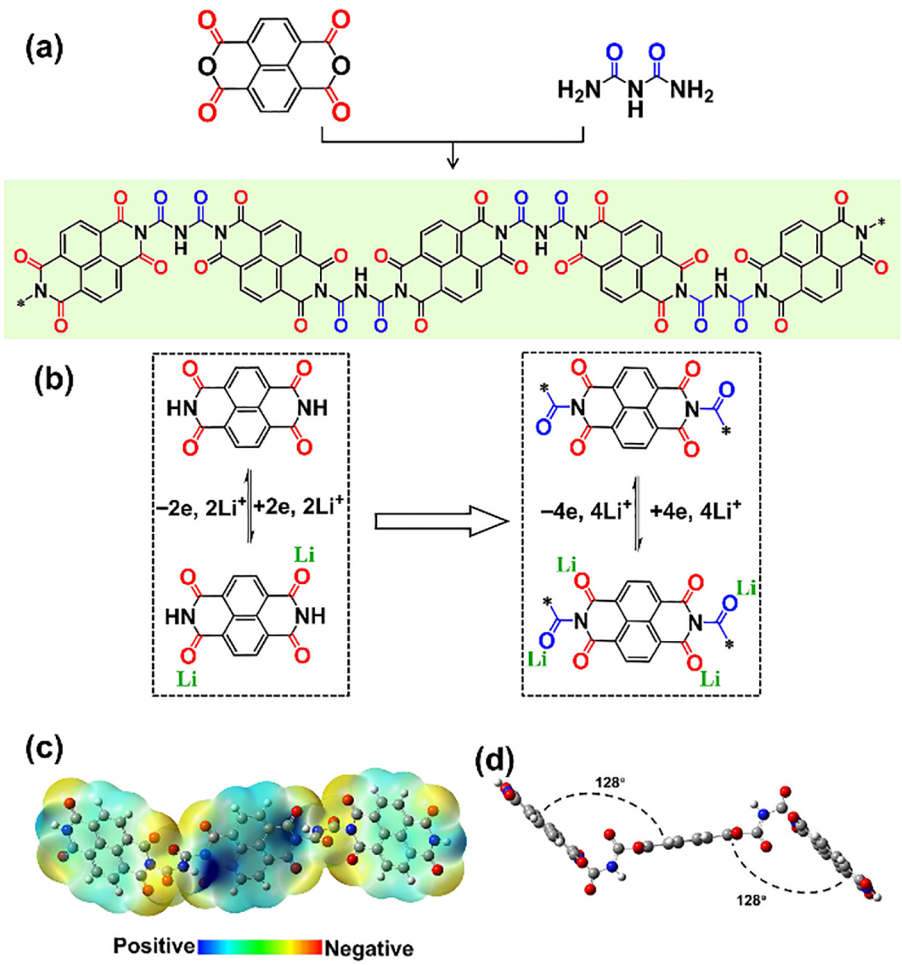

Figure 1 (a) Synthesis route to NDI-BU. (b) The 4-electron storage mechanism for NDI-BU unit. (c) ESP distribution of NDI-BU. (d) Molecular conformation of NDI-BU.

lithiation-delithiation. As depicted in Fig. 1(b), NDI unit can undergo a 2-electron redox reaction with lithium ions from 1.5 to 3.5 V voltage range. In order to achieve a multi-electron reaction, two carbonyl groups were connected to the nitrogen atoms in NDI unit. This p-π conjugation structure between NDI unit and carbonyl groups achieved a 4-electron redox reaction with lithium ions. Electrostatic potential (ESP) of NDI-BU shows that the first two lithium ions were anchored next to the oxygen atoms in NDI core unit. And the second two lithium ions were anchored next to the oxygen atoms in carbonyl groups which coming from biuret. Due to this 4-electron redox reaction, NDI-BU demonstrates a high specific capacity > 300 mAh·g^{-1} at 0.2C (theoretical capacity: 319 mAh·g^{-1}). This is the highest capacity among reported small organic molecules and polymers containing NDI/PDI groups [32]. Besides, NDI-BU shows a flat discharge plateau at 2.46 V versus Li^+/Li due to its non-conjugated structure. Remarkable cycle performance was also achieved with 93% capacity retention at 0.2C after 1000 cycles and 82% capacity retention at 5C after 20,000 cycles.

2 Experimental

2.1 Materials

N-methyl-2-pyrrolidone (NMP) and polyvinylidene fluoride (PVDF) were from Sigma Aldrich. 1,4,5,8-Naphthalenetetracarboxylic dianhydride was obtained from TCI. Dichloromethane, chloroform, tetrahydrofuran, acetone and dimethyl sulfoxide were provided by Aladdin. Ketjen black ECP600JD, electrolyte (1 M LiTFSI in DOL and DME, 1:1), Celgard2500 separator and lithium plate were obtained from DoDoChem. Carbon paper was obtained from Toray.

2.2 Synthesis of NDI-BU

Biuret (0.385 g, 3.73 mmol) and 1,4,5,8-naphthalene tetracarboxylic anhydride (1.0 g, 3.73 mmol) were added into a 100 mL flask. Imidazole (10 g) was added to the flask as solvent. Then, the mixture was stirred for 48 hours in nitrogen atmosphere at 140 °C and. 50 mL DMF was added to the hot reaction solution and filtered before cooling. The filter residue was washed by dichloromethane, chloroform, tetrahydrofuran, DMF, DMSO and acetone sequentially. The prepared product was dried in an oven at 100 °C for 10 hours. A pale-yellow solid was obtained (830 mg, 66%). ^{13}C solid-state NMR (600 MHz, δ): 165.9, 163.8, 130.4, 127.7, 124.6.

2.3 Material characterizations

FT-IR was tested on Thermo Nicolet 5700. TGA was performed by STA449F3 simultaneous thermal analyzer (25-600 °C, 10 °C·min^{-1}). The micromorphology characterization of the sample after gold spraying was performed by the JSM-6490LV instrument. XRD was measured on the D8 Advance

multifunction X-ray diffractometer (3°–70°). ^{13}C solid NMR was tested on Bruker NMR spectrometer (600 MHz). XPS was performed on Thermal Scientific ESCALAB 250Xi.

2.4 Preparation of electrodes and coin cell

A homogeneous slurry consisting of active polymer powder, Ketjen black and PVDF (weight ratio: 50:40:10) in NMP was grinded as the cathode material. Then, the slurry was coated on clean carbon paper (12 mm), and dried at 80 °C in an oven for 10 hours. The cathode loading of active material was 0.7–1.2 mg. Celgard 2500 membrane was used as the separator. Lithium sheet (14 mm) was used as the anode. After injecting the electrolyte, CR2032 coin-type cells were assembled in glovebox.

2.5 Electrochemical characterization

EIS and CV characterizations were tested on CHI-660E. For CV curves, the voltage range was 1.5–3.5 V, and the scanning rate was 0.2 $mV \cdot s^{-1}$. EIS plots were measured in a frequency range of 100–0.01 Hz, and the voltage amplitude was 5 mV. The charge and discharge profiles were tested on Neware battery testing system.

2.6 Electrical conductivity test

A two-probe test method was used to characterize the electronic conductivity of NDI-BU. The NDI-BU tablet (10 mm in diameter) was made by tableting machine at 200 MPa between two stainless steel sheets. The sandwich-like sample was encapsulated in Swagelok cell and tested using two-probe current-voltage technique.

2.7 DFT calculations

We selected three repeating units in the NDI-BU polymer for the calculation. Using Gaussian 09 program package, the polymer configuration and energy levels were calculated. The geometry was fully optimized with the B3LYP/6-31G (*d*, *p*) basis set.

3 Results and discussion

3.1 Synthesis and physicochemical characterization

NDI-BU was synthesized from 1,4,5,8napthalenetetracarboxylic acid dianhydride (NTCDA) and biuret (BU) through a polymerization reaction in imidazole at 140 °C for 48 h (Fig. 1(a). NDI-BU is difficult to dissolve in common organic solvents. The structure and properties of NDI-BU was characterized with thermal gravimetric analysis (TGA), solid-state ^{13}C nuclear magnetic resonance (NMR), X-ray diffraction (XRD), Fourier transform infrared spectroscopy (FT-IR), scanning electron microscopy (SEM), and X-ray photoelectron spectroscopy (XPS).

Solid-state ^{13}C NMR was performed to confirm the structure of NDI-BU (Fig. 2(a)). The peaks at 166 and 164 ppm correspond to the carbonyl carbon on the NDI and biuret units. The three peaks with chemical shifts between 120 and 140 ppm correspond to carbons at different positions on the naphthalene ring. The chemical states of the three elements were analyzed by high resolution XPS spectra (Fig. 2(b)). By fitting the C 1s XPS spectrum, four peaks at 288.1, 285.2, 284.8, and 284.3 eV were assigned to C=O, C-N, C=C (C-C), and C-H bonds. For O 1s and N 1s spectra, the binging energy at 531.5 and 400.1 eV can be attributed to C=O and C-N bonds. NDI-BU and the monomer NTCDA were also characterized with FT-IR (Fig. 2(c)). The absorption peak at 3180 cm^{-1} for NDI-BU is attributed to the N-H vibration from biuret. The absorption peaks of carbonyl group in NTCDA and NDI-BU are at 1761 and 1680 cm^{-1}. This absorption wavelength shift caused by the p-π conjugation structure between NDI unit and carbonyl groups. The aromatic anhydride ring vibration peak at 1516 cm^{-1} in NTCDA disappeared in NDI-BU due to anhydride ring opening and the formation of imide. The new peak at 1375 cm^{-1} in NDI-BU is attributed to the N-H bending vibration, and the new peak at 1349 cm^{-1} is attributed to stretching vibration of C-N. In addition, the stretching vibration peaks of C-O-C and C=O at 1154 and 1231 cm^{-1} in NTCDA disappeared in NDI-BU. These findings provide strong evidence of the polymerization reaction between biuret and NTCDA.

The morphology of NDI-BU was characterized with SEM (Fig. 2(d)). The image shows that NDI-BU has different size and irregular shape. The pores between the irregular micro-meter grains provide fast channels for the transmission of lithium ions. The porous structure of NDI-BU was characterized by nitrogen adsorption desorption measurement (Fig. S1 in the Electronic Supplementary Material (ESM)). NDI-BU shows reversible type-Ⅲ isotherms and a Brunauer-Emmett-Teller (BET) surface area of 5.8 $m^2 \cdot g^{-1}$ (Fig. S2 in the ESM). The reversible type-Ⅲ isotherms

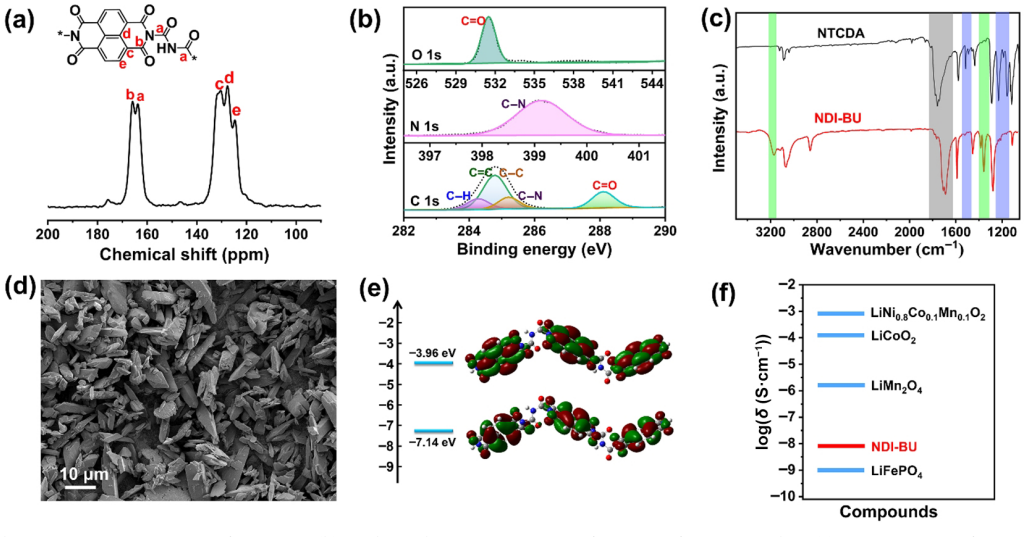

Figure 2 (a) Solid-state ^{13}C NMR spectrum of NDI-BU. (b) High resolution XPS spectra of NDI-BU for C, N, and O. (c) FT-IR spectra of NDI-BU and monomer NTCDA. (d) SEM image of NDI-BU. (e) The energy levels of NDI-BU. (f) Electrical conductivity of NDI-BU and selected inorganic electrode materials.

and a BET surface area of 5.8 $m^2 \cdot g^{-1}$ (Fig. S2 in the ESM). The average pore size and the dominant pore of NDI-BU is 9.25 and 1.66 nm. These micro-meter scale lithium ions transmission channels make it easier to charge and discharge at large current density, which is tested in the following section 3.2. The energy dispersive X-ray spectroscopy element mapping indicated that three elements C, N, and O are homogeneously distributed in the NDI-BU powder (Fig. S3 in the ESM). These characterizations provide more evidence that the NDI-BU polymer is formed. Furthermore, The TGA of NDI-BU shows good thermostability up to 400 °C (Fig. S4 in the ESM); and the XRD pattern indicates a good crystalline structure of NDI-BU (Fig. S5 in the ESM).

The energy levels of NDI-BU were calculated based on density functional theory (DFT) (Fig. 2(e)). Three repeat units terminated with hydrogen were chosen for DFT calculation. ESP was performed to predict the sites of reaction between NDI-BU and lithium ions (Fig. 1(c)). Among them, the lowest electrostatic potential is the easiest to reduce and combine with lithium ions. From the ESP map, the negative ESP values appeared near the carbonyl groups in the NDI and biuret units. The calculation results show that NDI-BU is not a co-planar structure, forming a zigzag configuration with a dihedral angle of 128° (Fig. 1(d)). The lowest unoccupied molecular orbital (LUMO) and the highest occupied molecular orbital (HOMO) energy levels of NDI-BU are −3.96 and −7.14 eV. The HOMO and LUMO orbitals break at the biuret units. As a result of this characteristics, there will not be any strong interactions between the redox units so that NDI-BU can exhibit flat discharge and charge plateaus. To further understanding the diffusion path in NDI-BU crystal, we calculated the molecular stacking in crystal structure by DFT. As shown in Fig. S6 in the ESM, due to the interaction of C-H-π, the distance between the two naphthalene rings is 6 Å. This distance is larger than the diameter of the lithium ion (1.2 Å). This regular hole can provide a fast diffusion path for lithium ions. Besides, oxygen atoms and nitrogen atoms along these holes provide abundant lithium-ion binding sites.

Furthermore, A two-probe test method was used to characterize the electronic conductivity of NDI-BU. Current-voltage curve of the NDI-BU tablet was carried from −0.5 to 0.5 V (Fig. S7 in the ESM). By measuring the thickness and diameter of the tablet, the conductivity of NDI-BU can be calculated to be about 1.1×10^{-8} $S \cdot cm^{-1}$. This conductivity is even higher than lithium iron phosphate, but far lower than the selected inorganic electrode materials in Fig. 2(f). The excellent electronic conductivity of NDI-BU may be attributed to ordered crystal structure formed by interaction of π-π between naphthalene diimide conjugated structure. High electronic conductivity is beneficial for the high-current charging and discharging of the battery.

3.2 CV curves and charge storage mechanism

The electrochemical properties of NDI-BU were analyzed in two-electrode setup using Li metal counter electrode. 1 M lithium bis(trifluoromethanesulphonyl) imide (LiTFSI) in DOL/DME (vol. ratio 1:1) was used as the electrolyte. NDI-BU electrodes are insoluble in the electrolyte (Fig. S8 in the ESM). Cyclic voltammetry (CV) was performed between 1.5 and 3.5 V with a scan rate of 0.2 $mV \cdot s^{-1}$. The CV curves of NDI-BU show four reversible redox peaks, suggesting that a multi-electron transfer reaction process (Fig. 3(a)). Except a minor shift of the cathodic peak at 2.4 V after the first cycle, these four redox couples overlap each other, suggesting that the multi-electron lithiation-delithiation processes of NDI-BU are stable. The first three galvanostatic charge and discharge curves of NDI-BU at 0.2C are displayed in Fig. 3(b) demonstrating a stable specific capacity at 308 $mAh \cdot g^{-1}$, which is very close to the theoretical capacity of 319 $mAh \cdot g^{-1}$. In order to exclude the influence of conductive carbon, we prepared batteries without NDI-BU. The result shows that conductive carbon contributes a specific capacity less than 5 $mAh \cdot g^{-1}$ (Fig. S9 in the ESM).

To shed the light on the Li storage mechanism, FT-IR was performed on NDI-BU after the full discharge and charge as displayed in Fig. 3(c). After fully discharged to 1.5 V versus Li^+/Li, two new peaks at 1402 and 1556 cm^{-1} emerged comparing to the pristine NDI-BU. The new peak at 1402 cm^{-1} can be attributed to C-O single bond formed by the electrochemical reduction of C=O double bonds, which is evidenced by the diminished C=O peaks around 1700 cm^{-1}. The new peak at 1556 cm^{-1} can be attributed to C=N double bond from C-N single bond formed by the reduction of the neighboring C=O group. When NDI-BU is charged back to

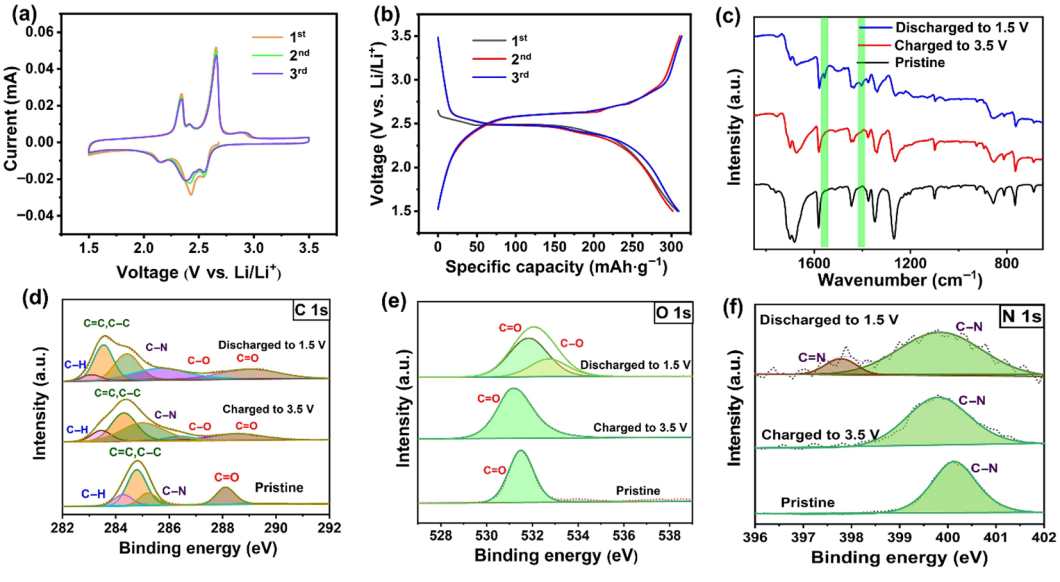

Figure 3 (a) The first three CV cycles. (b) The first three charge and discharge curves at 0.2C. (c) The *ex-situ* FT-IR spectra of the NDI-BU electrode at pristine, first discharged and fully charged. (d)–(f) The *ex-situ* local scan XPS spectra of C 1s, O 1s and N 1s at pristine, first discharged and fully charged.

3.5 V, these two peaks disappeared and the intensity of the C=O peak is enhanced, which indicates the good reversibility of the reduction of NDI-BU. XPS analysis provides additional evidence of the reversible redox mechanism. As shown in the spectra of C 1s in Fig. 3(d), the C-O bond at 285.8 eV appears after NDI-BU discharged to 1.5 V, accompanied by the diminishing of the C=O peak. It is consistent with the emerging C-O peak in the O 1s spectra at 532.7 eV in Fig. 3(e). We also observed a new C=N bond at 398 eV after discharge process from the local scan spectra for the N 1s (Fig. 3(f). These results prove that the reaction between carbonyl group and lithium ion occurs. Besides, *ex-situ* XRD of NDI-BU electrode at pristine, 1st discharged and charged were investigated (Fig. S10 in the ESM). After discharged and charged, there were only two main diffraction peaks left compared to pristine state, indicating that lithiation and delithiation process reduced the ordering of crystals. But the similar shape of discharged and charged XRD diffraction demonstrated that the stability of NDI-BU crystal structure.

3.3 Electrochemical performance

In addition to high specific capacity, NDI-BU also demonstrates excellent cycle stability as displayed in Fig. 4(a). The capacity at 0.2C was retained at 273 mAh·g^{-1} even after 1000 cycles with a capacity retention of 93%. We also tested the rate performance of NDI-BU. As shown in Figs. 4(b) and 4(c), the discharge capacities of NDI-BU at 0.2C, 0.5C, 1C, 2C, 5C, and 10C are 303, 288, 278, 269, 258, and 251 mAh·g^{-1} respectively. Furthermore, the polarization of the charge-discharge curve at different current density is very small, and the shape maintains similar. At 10C, there is still a capacity retention of 83%. The capacity still remains 290 mAh·g^{-1} when the current returns to 0.2C, and the capacity recovery ratio is 96%. We performed a high-rate, long-cycle stability test at 5C (Fig. 4(d)), the first discharge capacity is 276 mAh·g^{-1}, and excellent cycle performance was achieved with 82% capacity retention after 20,000 cycles. Around 100% of the Coulombic efficiency is maintained during these cycles. This excellent cycle stability surpasses most organic imide cathode materials reported in LIBs (Fig. 4(e), Table S1 in the ESM).

Based on the excellent high-current charge-discharge performance of ND-BU electrode materials, we tested the rate performance with different conductive carbon ratios and high loadings (Figs. S11 and S13 in the ESM). When the ratio of NDI-BU, Ketjen black and PVDF increased to 6:3:1, the initial discharge specific capacity of the battery is 210 mAh·g^{-1}. With the increase of charge-discharge current density, the discharge specific capacity dropped to 193 mAh·g^{-1} at 10C, maintaining a capacity retention of 91%. When the ratio of NDI-BU, Ketjen black and PVDF increased to 7:2:1, a similar rate performance was obtained compared to 6:3:1. The initial discharge specific capacity dropped to 170 mAh·g^{-1} when the content of active material reaching up to 8:1:1. In the ratio comparable to inorganic battery materials, NDI-BU still shows excellent capacity and rate performance. To further understanding the electrochemical performance of NDI-BU with a ratio of 6:3:1, we tested CV cycle and long-cycle stability (Fig. S12 in the ESM). The CV curve shows more redox peaks compared to the ratio of 5:4:1. Charge and discharge profiles at different current densities indicate that NDI-BU has a stable charging and discharging platform. At 0.5C and 5C with a ratio of 6:3:1, NDI-BU also shows excellent stability after 100 and 500 cycles. These test results prove the practical application significance of NDI-BU. When the mass loadings of NDI-BU came to 5.7 and 10.7 mg, The initial capacity were reduced to 176 and 148 mAh·g^{-1}. Under high current rate, charge and discharge capacity were greatly decreased to 70 mAh·g^{-1}.

Figure 4(f) shows the electrochemical impedance spectroscopy (EIS) at initial and 500th cycle. The fitting line displays from middle to low frequencies indicate the diffusion process of lithium ions, and the fitting semi-circular shape at high frequencies shows charge transfer process. The equivalent circuit is shown in Fig. S14 in the ESM, and Warburg impedance (*W*), electrolyte resistance (*Rs*), and charge transfer resistance (*Rct*) are compared in Table S2 in the ESM. *W* decreased slightly from 56 to 42 Ω after 500 cycles. *Rs* and *Rct* were 1.89, 105.6 Ω and 1.92, 102.7 Ω after 1st and 500th cycles. To understanding the decreasing of *Rct* after long cycle, we tested the CV curves after the 1st, 10th and 500th cycles (Fig. S15 in the ESM). With the number of cycles increasing, the oxidation peaks shift to the low potential, and the reduction peaks shift to the high potential. This result indicated that the reversibility of the battery was improved, and *Rct* was reduced. We further investigate the morphology change of the NDI-BU cathode during discharge and charge processes (Fig. S16 in the ESM). The *ex-situ* SEM images show that there was no obvious

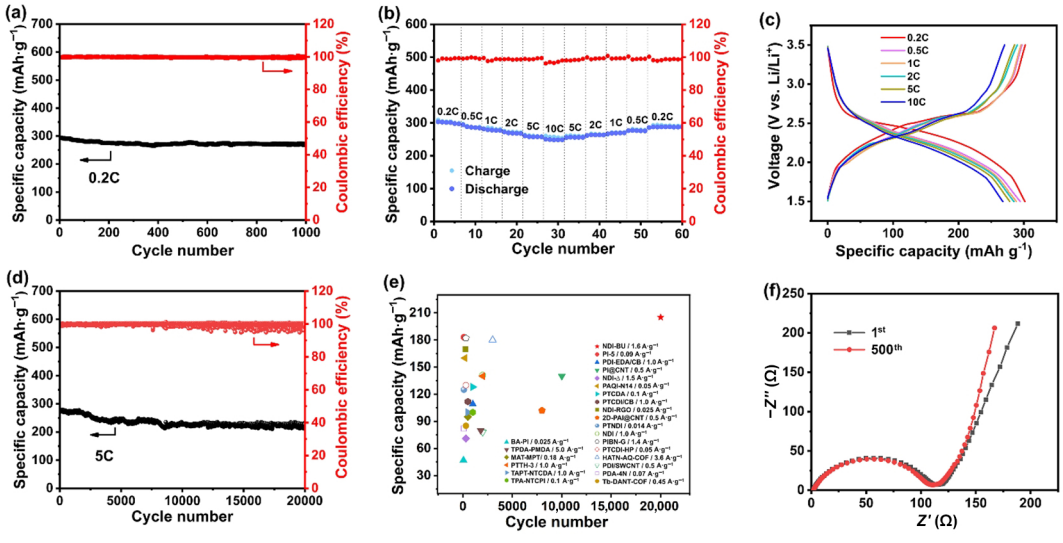

Figure 4 (a) and (d) Stability of long-term cycles at 0.2C and 5C. (b) Rate performance. (c) Charge and discharge profiles at different current densities. (e) Comparison of long cycle performance of NDI-BU versus previously reported imide-containing cathodes for LIBs. (f) Nyquist plots after the first and 500th cycle.

morphology change and exfoliation of NDI-BU during the long cycle. These results indicate that the electrode has a very stable kinetic process and morphology during cycling.

3.4 Kinetics of NDI-BU cathode

Through CV measurements, the charge and discharge kinetics of NDI-BU cathode were investigated (Fig. 5(a)). In general, the equation $i = av^b$ can be used to describe the relationship between the sweep rate (v) and the peak current (i) [33]. When the b value is close to 0.5, the oxidation or reduction reaction is a diffusion control process. When the b value is close to 1.0, the corresponding reaction is a pseudocapacitance process. For the NDI-BU electrode, the b values of the five reversible redox peaks O_1, O_2, R_1, R_2, and R_3 are 0.83, 0.5, 0.8, 0.72, and 0.72 respectively (Fig. 5(b)). The result indicate that O_2 is a diffusion control process, and the rest redox reactions are dominated by both capacitive and diffusion processes. The diffusion and capacitive controlled processes in the NDI-BU electrode can be quantitatively analyzed by the following equation: $i = k_1v + k_2v^{0.5}$. The contributions of the capacitance and diffusion processes are shown in Fig. 5(c). When the scan rate increases from 0.1 to 0.8 mV·s^{-1}, the capacitive control process ratio increases from 82.2% to 92.3%. The highly capacitive contribution might be significantly influenced by the random shape with different size of NDI-BU [34].

The lithium-ion diffusion in NDI-BU electrode was studied through galvanostatic intermittent titration (GITT) method (Figs. S17 and S18 in the ESM). The calculated lithium-ion diffusion coefficient was 10^{-10} to 10^{-9} cm^2·s^{-1}, higher than most conventional inorganic cathode materials [35]. The pores between the irregular micro-meter grains provide fast channels for the transmission of lithium ions.

3.5 DFT simulation of the lithiated NDI-BU

The optimized structures of NDI-BU during the lithiation and delithiation processes were calculated. Figure 6(a) shows the change of discharge curve in different lithiation states from NDI-BU to NDI-BU-xLi (x = 1, 2, 3, 4). It is clear that each lithiation state corresponds to a discharge plateau. The total energy shows small decreasing from NDI-BU to NDI-BU-4Li, indicateing that NDI-BU has a long and flat discharge platform. Calculations show that each repeat unit can undergo redox reactions with four lithium ions and four electrons (Fig. 6(b)). The first two lithium ions are combined with carbonyl groups in the NDI moiety, and the rest two lithium ions react with carbonyl groups in biuret moiety. The four-electron redox reaction site makes the theoretical capacity NDI-BU polymer at 319 mAh·g^{-1}, which agrees well with the demonstrated 308 mAh·g^{-1} capacity under 0.2C.

4 Conclusion

In summary, a novel multi-carbonyl naphthalene diimide polymer

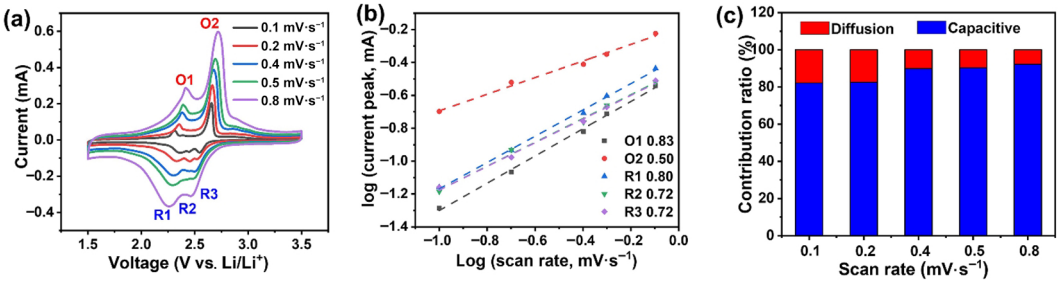

Figure 5 Kinetics analyses of NDI-BU electrode. (a) CV curves. (b) Fitting line of log(v) versus log(i) and the b values. (c) The contributions of diffusion and capacitive controlled process.

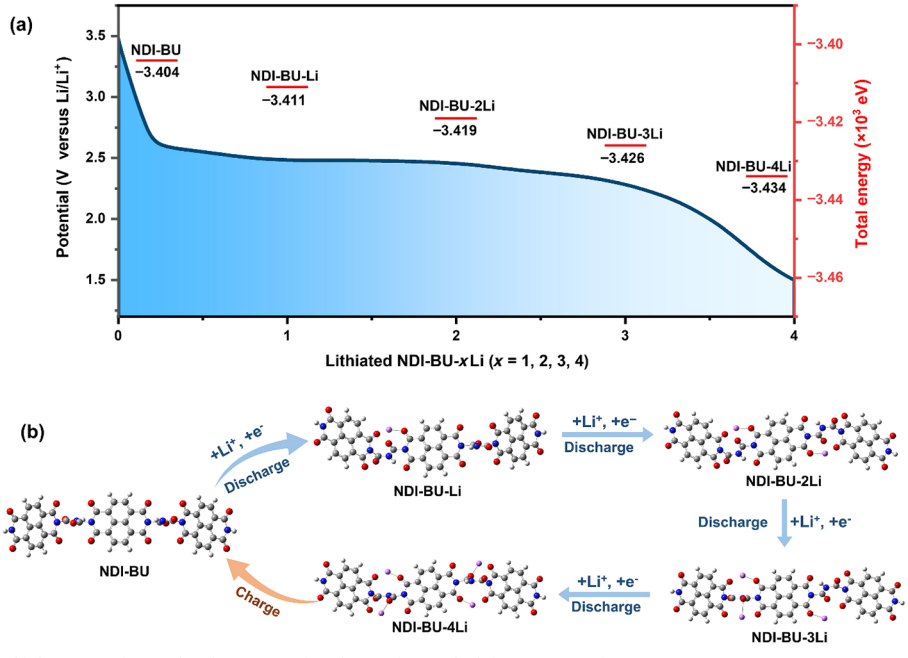

Figure 6 (a) The simulated lithiation pathway. (b) The structural evolution during the lithiation procedure.

have been synthesized for stable lithium-ion storage. The NDI-BU is characterized by abundant redox-active carbonyl centers, non-conjugated polymer backbone and high structure stability, which enable high capacity and long discharge plateau. Notably, NDI-BU exhibits remarkable rate performance and excellent cycle life based on crystal structure stability and cathode insolubility in electrolyte. The lithium-ion storage in NDI-BU is revealed as a fast pseudocapacitive process. DFT calculation shows that NDI-BU undergoes a four-electron redox reaction per repeat unit, which was revealed by *ex-situ* FT-IR, XPS and XRD characterizations during charging and discharging. These results provide an effective design strategy for multi-carbonyl organic LIB cathode materials.

Acknowledgements

We appreciate the support from the National Natural Science Foundation of China (Nos. 22075255， 22375080, and 22175081), Co-working Space Incubation Project of Zhengzhou University of Light Industry (No. 2021ZCKJ209), Science and Technology Project of Henan Province (No. 242102240007), Key Scientific Research Project of Henan Province (No. 25A530007), the Education Department of Henan Province (No. 242300420206), and the Science and Technology Major Program of Gansu Province of China (Nos. 22ZD6FA006, 23ZDFA015, and 24ZD13FA017).

Declaration of conflicting interests

The authors declare no conflicting interests regarding the content of this article.

Data availability

All data needed to support the conclusions in the paper are presented in the manuscript and/or the Supplementary Materials. Additional data related to this paper may be requested from the corresponding author upon request.

Electronic Supplementary Material: Supplementary material (N_2 adsorption-desorption isotherms, EDX analysis, TGA spectra, XRD patterns, molecular stacking analysis, electronic conductivity test, solubility test of BDI-BU, rate performance with different conductive carbon ratios and high loadings, electrochemical performance of NDI-BU with a ratio of 6:3:1, CV curves after the 1st, 10th and 500th cycles, SEM images and GITT profiles) is available in the online version of this article at https://doi.org/10.26599/NRE.2025.9120159.

References

[1] Ye, H. L.; Li, Y. G. Towards practical lean-electrolyte Li–S batteries: Highly solvating electrolytes or sparingly solvating electrolytes. *Nano Res. Energy* **2022**, *1*, e9120012.

[2] Wu, X. X.; Ji, G. J.; Wang, J. X.; Zhou, G. M.; Liang, Z. Toward sustainable all solid-state Li-metal batteries: Perspectives on battery technology and recycling processes. *Adv. Mater.* **2023**, *35*, 2301540.

[3] Wan, H. L.; Wang, Z. Y.; Zhang, W. R.; He, X. Z.; Wang, C. S. Interface design for all-solid-state lithium batteries. *Nature* **2023**, *623*, 739–744.

[4] Su, H.; Chen, Z. F.; Li, M. J.; Bai, P. X.; Li, Y.; Ji, X.; Liu, Z. Q.; Sun, J.; Ding, J.; Yang, M. et al. Achieving practical high-energy-density lithium-metal batteries by a dual-anion regulated electrolyte. *Adv. Mater.* **2023**, *35*, 2301171.

[5] Liu, Y. Y.; Shi, H. D.; Wu, Z. S. Recent status, key strategies and challenging perspectives of fast-charging graphite anodes for lithium-ion batteries. *Energy Environ. Sci.* **2023**, *16*, 4834–4871.

[6] She, P. F.; Qin, Y. Y.; Wang, X.; Zhang, Q. C. Recent progress in external-stimulus-responsive 2D covalent organic frameworks. *Adv. Mater.* **2022**, *34*, 2101175.

[7] Song, Z. Y.; Chen, F. F.; Martinez-Ibañez, M.; Feng, W. F.; Forsyth, M.; Zhou, Z. B.; Armand, M.; Zhang, H. A reflection on polymer electrolytes for solid-state lithium metal batteries. *Nat. Commun.* **2023**, *14*, 4884.

[8] Wen, X. Y.; Zhang, J.; Luo, H. W.; Shi, J. Y.; Tsay, C.; Jiang, H. H.; Lin, Y. H.; Schroeder, M. A.; Xu, K.; Guo, J. C. Synthesis and electrochemical properties of aluminum hexafluorophosphate. *J. Phys. Chem. Lett.* **2021**, *12*, 5903–5908.

[9] Zhang, G. Z.; Chang, J.; Wang, L. G.; Li, J. W.; Wang, C. Y.; Wang, R.; Shi, G. L.; Yu, K.; Huang, W.; Zheng, H. H. et al. A monofluoride ether-based electrolyte solution for fast-charging and low-temperature non-aqueous lithium metal batteries. *Nat. Commun.* **2023**, *14*, 1081.

[10] Wang, Y. K.; Li, Z. M.; Hou, Y. P.; Hao, Z. M.; Zhang, Q.; Ni, Y. X.; Lu, Y.; Yan, Z. H.; Zhang, K.; Zhao, Q. et al. Emerging electrolytes with fluorinated solvents for rechargeable lithium-based batteries. *Chem. Soc. Rev.* **2023**, *52*, 2713–2763.

[11] Lu, Y.; Chen, J. Prospects of organic electrode materials for practical lithium batteries. *Nat. Rev. Chem.* **2020**, *4*, 127–142.

[12] Zhu, Y. H.; Yang, X. Y.; Liu, T.; Zhang, X. B. Flexible 1D batteries: Recent progress and prospects. *Adv. Mater.* **2020**, *32*, 1901961.

[13] Wang, G.; Chandrasekhar, N.; Biswal, B. P.; Becker, D.; Paasch, S.; Brunner, E.; Addicoat, M.; Yu, M. H.; Berger, R.; Feng, X. L. A crystalline, 2D polyarylimide cathode for ultrastable and ultrafast Li storage. *Adv. Mater.* **2019**, *31*, 1901478.

[14] Lu, Y.; Hou, X. S.; Miao, L. C.; Li, L.; Shi, R. J.; Liu, L. J.; Chen, J. Cyclohexanehexone with ultrahigh capacity as cathode materials for lithium-ion batteries. *Angew. Chem., Int. Ed.* **2019**, *58*, 7020–7024.

[15] Peng, C. X.; Ning, G. H.; Su, J.; Zhong, G. M.; Tang, W.; Tian, B. B.; Su, C. L.; Yu, D. Y.; Zu, L. H.; Yang, J. H. et al. Reversible multi-electron redox chemistry of π-conjugated N-containing heteroaromatic molecule-based organic cathodes. *Nat. Energy* **2017**, *2*, 17074.

[16] Petronico, A.; Bassett, K. L.; Nicolau, B. G.; Gewirth, A. A.; Nuzzo, R. G. Toward a four-electron redox quinone polymer for high capacity lithium ion storage. *Adv. Energy Mater.* **2018**, *8*, 1700960.

[17] Jiang, Q.; Xiong, P. X.; Liu, J. J.; Xie, Z.; Wang, Q. C.; Yang, X. Q.; Hu, E. Y.; Cao, Y.; Sun, J.; Xu, Y. H. et al. A redox-active 2D metal-organic framework for efficient lithium storage with extraordinary high capacity. *Angew. Chem., Int. Ed.* **2020**, *59*, 5273–5277.

[18] Wang, H.; Yao, C. J.; Nie, H. J.; Wang, K. Z.; Zhong, Y. W.; Chen, P. W.; Mei, S. L.; Zhang, Q. C. Recent progress in carbonyl-based organic polymers as promising electrode materials for lithium-ion batteries (LIBs). *J. Mater. Chem. A* **2020**, *8*, 11906–11922.

[19] Yang, X. Y.; Gong, L.; Liu, X. L.; Zhang, P. P.; Li, B. W.; Qi, D. D.; Wang, K.; He, F.; Jiang, J. Z. Mesoporous polyimide-linked covalent organic framework with multiple redox-active sites for high-performance cathodic Li storage. *Angew. Chem., Int. Ed.* **2022**, *61*, e202207043.

[20] Liang, Y. L.; Chen, Z. H.; Jing, Y.; Rong, Y. G.; Facchetti, A.; Yao, Y. Heavily n-dopable π-conjugated redox polymers with ultrafast energy storage capability. *J. Am. Chem. Soc.* **2015**, *137*, 4956–4959.

[21] Yang, P.; Xi, X.; Huang, T.; Zhong, Q. Q.; Jiang, B.; Liu, R. L.; Wu, D. Q. An acid-assisted vacuum filtration approach towards flexible PDI/SWCNT cathodes for highly stable organic lithium ion batteries. *Electrochim. Acta* **2020**, *338*, 135771.

[22] Luo, H. W.; Liu, Z. T. Recent developments of di-amide/imide-containing small molecular non-fullerene acceptors for organic solar cells. *Chin. Chem. Lett.* **2016**, *27*, 1283–1292.

[23] Yao, M. S. R.; Taguchi, N.; Ando, H.; Takeichi, N.; Kiyobayashi, T.

Improved gravimetric energy density and cycle life in organic lithium-ion batteries with naphthazarin-based electrode materials. *Commun. Mater.* **2020**, *1*, 70.
[24] Huang, W. W.; Zheng, S. B.; Zhang, X. Q.; Zhou, W. J.; Xiong, W. X.; Chen, J. Synthesis and application of calix[6]quinone as a high-capacity organic cathode for plastic crystal electrolyte-based lithium-ion batteries. *Energy Storage Mater.* **2020**, *26*, 465–471.
[25] Wang, Y. Q.; Bai, P. X.; Li, B. F.; Zhao, C.; Chen, Z. F.; Li, M. J.; Su, H.; Yang, J. X.; Xu, Y. H. Ultralong cycle life organic cathode enabled by ether-based electrolytes for sodium-ion batteries. *Adv. Energy Mater.* **2021**, *11*, 2101972.
[26] Luo, H. W.; Liu, Z. T.; Zhang, D. Q. Conjugated D-A terpolymers for organic field-effect transistors and solar cells. *Polym. J.* **2018**, *50*, 21–31.
[27] Wang, S. W.; Wang, L. J.; Zhang, K.; Zhu, Z. Q.; Tao, Z. L.; Chen, J. Organic $Li_4C_8H_2O_6$ nanosheets for lithium-ion batteries. *Nano Lett.* **2013**, *13*, 4404–4409.
[28] Luo, H. W.; Dong, X. B.; Cai, Z. X.; Wang, L. Z.; Liu, Z. T. Pechmann dye-based molecules containing fluorobenzene moieties for ambipolar organic semiconductors. *Asian J. Org. Chem.* **2018**, *7*, 592–597.
[29] Bhosale, M. E.; Chae, S.; Kim, J. M.; Choi, J. Y. Organic small molecules and polymers as an electrode material for rechargeable lithium ion batteries. *J. Mater. Chem. A* **2018**, *6*, 19885–19911.
[30] Luo, H. W.; He, D. D.; Zhang, Y.; Wang, S. W.; Gao, H. L.; Yan, J.; Cao, Y.; Cai, Z. X.; Tan, L. X.; Wu, S. D. et al. Synthesis of heterocyclic core-expanded bis-naphthalene tetracarboxylic diimides. *Org. Lett.* **2019**, *21*, 9734–9737.
[31] Kim, J.; Kim, Y.; Yoo, J.; Kwon, G.; Ko, Y.; Kang, K. Organic batteries for a greener rechargeable world. *Nat. Rev. Mater.* **2023**, *8*, 54–70.
[32] Biradar, M. R.; Bhosale, S. V.; Morajakar, P. P.; Bhosale, S. V. A review on energy storage devices based on rylene imide dyes: Synthesis, applications and challenges. *Fuel* **2022**, *310*, 122487.
[33] Lee, S.; Kwon, G.; Ku, K.; Yoon, K.; Jung, S. K.; Lim, H. D.; Kang, K. Recent progress in organic electrodes for Li and Na rechargeable batteries. *Adv. Mater.* **2018**, *30*, 1704682.
[34] An, Y. K.; Liu, Y.; Tan, S. S.; Xiong, F. Y.; Liao, X. B.; An, Q. Y. Dual redox groups enable organic cathode material with a high capacity for aqueous zinc-organic batteries. *Electrochim. Acta* **2022**, *404*, 139620.
[35] Chien, Y. C.; Liu, H. D.; Menon, A. S.; Brant, W. R.; Brandell, D.; Lacey, M. J. Rapid determination of solid-state diffusion coefficients in Li-based batteries via intermittent current interruption method. *Nat. Commun.* **2023**, *14*, 2289.

Hewei Luo received Ph.D degree from Institute of Chemistry, Chinese Academy of Sciences in 2015. He is currently an associate professor at Zhengzhou University of Light Industry since 2015. His current researches focus on the design and synthesis of functional materials for lithium-ion, sodium-ion and zinc-ion batteries.

Juchen Guo is currently a Professor in the Department of Chemical and Environmental Engineering and the Chair of the Materials Science and Engineering Program at the University of California – Riverside (UCR). He also serves as the co-director of Winston Chung Global Energy Center at UCR. His research interests focus on the interfacial phenomena and material properties in electrochemical energy storage systems including lithium metal, lithium-sulfur, and multivalent-ion batteries such as magnesium and aluminum systems. Juchen Guo earned his Bachelor degree in chemical engineering from Zhejiang University in 1999 and his Ph.D. in chemical engineering from University of Maryland in 2007. He held postdoctoral positions at University of Maryland from 2007 to 2011 and Cornell University from 2011 to 2012 prior to joining UCR in 2012. He was the recipient of 2014 Hellman Fellowship and 2018 NSF CAREER Award.

Zitong Liu received Ph.D degree from Institute of Chemistry, Chinese Academy of Sciences in 2008. He is currently a professor at Lanzhou University, China. He is interested in developing new organic functional materials for electronic and optoelectronic applications.